


 Cite this: *RSC Adv.*, 2019, **9**, 16195

Catalytic effect of $(\text{H}_2\text{O})_n$ ($n = 1\text{--}3$) clusters on the $\text{HO}_2 + \text{SO}_2 \rightarrow \text{HOSO} + {}^3\text{O}_2$ reaction under tropospheric conditions†

Rui Wang, *^a Qiuyue Yao, ^{†,b} Mingjie Wen, ^{†,a} Shaobo Tian, ^{†,a} Yan Wang, ^{†,a} Zhiyin Wang, ^a Xiaohu Yu, ^a Xianzhao Shao^a and Long Chen^{cd}

The $\text{HO}_2 + \text{SO}_2 \rightarrow \text{HOSO} + {}^3\text{O}_2$ reaction, both without a catalyst and with $(\text{H}_2\text{O})_n$ ($n = 1\text{--}3$) as a catalyst, has been investigated using CCSD(T)/CBS//M06-2X/aug-cc-pVTZ methods, and canonical variational transition state theory with small curvature tunneling (CVT/SCT). The calculated results show that H_2O exerts the strongest catalytic role in the hydrogen atom transfer processes of $\text{HO}_2 + \text{SO}_2 \rightarrow \text{HOSO} + {}^3\text{O}_2$ as compared with $(\text{H}_2\text{O})_2$ and $(\text{H}_2\text{O})_3$. In the atmosphere at 0 km altitude within the temperature range of 280.0–320.0 K, the reaction with H_2O is dominant, compared with the reaction without a catalyst, with an effective rate constant 2–3 orders of magnitude larger. In addition, at 0 km, it is worth mentioning that the relevance of the $\text{HO}_2 + \text{SO}_2 \rightarrow \text{HOSO} + {}^3\text{O}_2$ reaction with H_2O depends heavily on its ability to compete with the primary loss mechanism of HO_2 radicals (such as the $\text{HO}_2 + \text{HO}_2$ and $\text{HO}_2 + \text{NO}_3$ reactions) and SO_2 (such as the $\text{SO}_2 + \text{HO}$ reaction). The calculated results show that the $\text{HO}_2 + \text{SO}_2 \rightarrow \text{HOSO} + {}^3\text{O}_2$ reaction with H_2O cannot be neglected in the primary loss mechanism of the HO_2 radical and SO_2 . The calculated results also show that for the formation of HOSO and ${}^3\text{O}_2$, the contribution of H_2O decreases from 99.98% to 27.27% with an increase in altitude from 0 km to 15 km, due to the lower relative concentration of water. With the altitude increase, the $\text{HO}_2 + \text{SO}_2 \rightarrow \text{HOSO} + {}^3\text{O}_2$ reaction with H_2O cannot compete with the primary loss mechanism of HO_2 radicals. The present results provide new insight into $(\text{H}_2\text{O})_n$ ($n = 1\text{--}3$) catalysts, showing that they not only affect energy barriers, but also have an influence on loss mechanisms. The present findings should have broad implications in computational chemistry and atmospheric chemistry.

Received 8th January 2019
Accepted 2nd May 2019

DOI: 10.1039/c9ra00169g
rsc.li/rsc-advances

1. Introduction

As a significant gaseous pollutant from both industrial and natural sources,¹ sulfur dioxide (SO_2)^{2,3} can cause a wide range of issues for human health, agriculture and the global climate.⁴ It leads to acid rain that damages forest and crops, and plays a role in the formation of atmospheric aerosols.^{5,6} Furthermore, short-term exposure to high levels of SO_2 in the air can be life-

threatening, as it can cause breathing difficulties and obstruct airways, while long-term exposure to persistent levels of SO_2 can cause chronic bronchitis, emphysema and respiratory illness.⁷ Similar to SO_2 , the hydroperoxyl radical (HO_2) is also an important atmospheric species, which plays important roles in both the troposphere and the stratosphere.⁸ In the troposphere, the HO_2 radical is central to the production of ozone and the generation of hydroxyl radicals, whereas in the stratosphere, it is involved in catalytic cycles. HO_2 also acts as a significant transient intermediate in the combustion of hydrocarbon fuels, atmospheric photolysis cycles, and biochemical processes.^{9,10} The reaction between HO_2 and SO_2 has aroused great interest from many research groups due to its great importance to supply a reverse path between SO_2 and HOSO (or SO_3) in the sulfur cycle. This reaction may take place *via* a number of pathways including the three main product paths shown in eqn (1)–(3), namely, $\text{O}_2 + \text{HOSO}$ formation, $\text{O}_2 + \text{HSO}_2$ formation, and $\text{OH} + \text{SO}_3$ formation.^{3,11} It is noteworthy that, as one of the most important products of the $\text{HO}_2 + \text{SO}_2$ reaction, HOSO has been found to be relatively stable¹² and its subsequent reactions¹³ are important for atmospheric chemistry. Therefore, its structure,^{14,15} harmonic vibrational frequencies,¹⁶

^aShaanxi Key Laboratory of Catalysis, School of Chemical & Environment Science, Shaanxi University of Technology, Hanzhong, Shaanxi, P. R. China. E-mail: wangrui830413@163.com; Fax: +86-0916-2641083; Tel: +86-0916-2641083

^bHenan Key Laboratory of Boron Chemistry and Advanced Energy Materials, School of Chemistry and Chemical Engineering, Henan Normal University, Xinxiang, Henan 453007, China

^cKey Lab of Aerosol Chemistry & Physics, Institute of Earth Environment, Chinese Academy of Sciences, Xi'an, Shaanxi, P. R. China

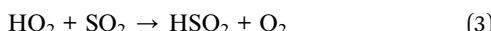
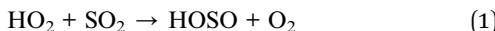
^dState Key Laboratory of Loess and Quaternary Geology, Institute of Earth Environment, Chinese Academy of Sciences, Xi'an, Shaanxi, P. R. China

† Electronic supplementary information (ESI) available. See DOI: 10.1039/c9ra00169g

‡ Qiuyue Yao, Mingjie Wen, Shaobo Tian, and Yan Wang contributed equally to this work.



thermochemistry^{12,17} and subsequent reactions^{13,18} have been widely investigated.



The kinetics and mechanism of the $\text{HO}_2 + \text{SO}_2$ reaction have been studied experimentally and theoretically for a range of temperatures and pressures. In an experimental study, Payne *et al.*¹⁹ found that the rate constant of the $\text{HO}_2 + \text{SO}_2$ reaction was $(8.7 \pm 1.8) \times 10^{-16} \text{ cm}^3$ per molecule per s at 300 K and a pressure of 30 Torr. Meanwhile, the rate constant of the $\text{HO}_2 + \text{SO}_2$ reaction at 298 K was found to be $2.01 \times 10^{-17} \text{ cm}^3$ per molecule per s, as measured by Burrows *et al.*²⁰ at low pressure. The kinetics and mechanism for the reaction of HO_2 with SO_2 were investigated by Wang *et al.*¹¹ with *ab initio* molecular orbital and transition state theory calculations. Their results showed that the reaction firstly proceeds to form a five-membered ring complex $\text{SO}_2 \cdots \text{HO}_2$, and then the complex undergoes barrierless decomposition to produce $\text{O}_2 + \text{HOSO}$. These investigations provide meaningful information about the mechanisms and kinetics for the $\text{HO}_2 + \text{SO}_2$ reaction under atmospheric conditions. However, this effort has only focused on the non-catalytic process of the $\text{HO}_2 + \text{SO}_2$ reaction.

Water has long been considered as a subject of chemical interest due to its abundance and unique properties in atmospheric chemistry.²¹ It not only forms hydrogen-bonded complexes with HO_2 ,^{22,23} OH ,^{24–26} formic acid²¹ and nitric acid,⁸ but also can actively participate in atmospheric reactions as a catalyst,^{27,28} of which $\text{HO}_2 \cdots \text{H}_2\text{O}$ is a well-studied example.^{29–31} An interesting result²⁹ concerning this complex is that the HO_2 self-reaction can be up to three times faster in the presence of water, since 30% of HO_2 radicals may exist in the form of $\text{HO}_2 \cdots \text{H}_2\text{O}$.³² Moreover, many experimental and theoretical studies have been reported on the electronic structure of the clusters $\text{SO}_2 \cdots \text{H}_2\text{O}$ ^{33–37} and the gaseous hydrolysis reaction of $\text{SO}_2 + \text{H}_2\text{O}$.^{3,11} These situations stimulated our interest in modeling the gas-phase reaction of the $\text{H}_2\text{O} \cdots \text{HO}_2 \cdots \text{SO}_2$ ternary system, in which a single water molecule serves as a catalyst.

Recently, Chen *et al.*³ employed the CCSD(T)/aug-cc-pVTZ//B3LYP/aug-cc-pVTZ method to investigate the reactions of $\text{HO}_2 + \text{SO}_2$ and $\text{HO}_2 \cdots \text{H}_2\text{O} + \text{SO}_2$. Their calculations showed that H_2O slightly accelerates the $\text{SO}_2 + \text{HO}_2$ reaction to form a $\text{HSO}_4 \cdots \text{H}_2\text{O}$ radical complex. Although Chen *et al.*³ provided meaningful information on the mechanism and kinetics of $\text{HO}_2 \cdots \text{H}_2\text{O} + \text{SO}_2$ and $\text{HO}_2 + \text{SO}_2$ reactions under tropospheric conditions, the most favorable, water-assisted channel ($\text{HO}_2 + \text{SO}_2 \rightarrow \text{HOSO} + \text{O}_2$) has not yet been investigated in this way. Thus, it is still difficult to judge whether water molecules have an obvious positive catalytic effect on the $\text{HO}_2 + \text{SO}_2$ reaction or not. Furthermore, many experimental and theoretical studies have appeared in the literature on the electronic structure of the clusters $\text{HO}_2 \cdots (\text{H}_2\text{O})_n$ ($n = 2–3$)^{38,39} and $\text{SO}_2 \cdots (\text{H}_2\text{O})_n$ ($n = 2–3$).^{40,41} On the other hand, some studies have shown that water

dimers^{38,42–49} and trimers^{39,49–52} can also have a significant catalytic effect in hydrogen abstraction reactions and hydrolysis of sulfur dioxide.^{53,54} Thus, the investigation of the effect of $(\text{H}_2\text{O})_n$ ($n = 1–3$) on the $\text{HO}_2 + \text{SO}_2 \rightarrow \text{HOSO} + {}^3\text{O}_2$ reaction is a logical path to pursue.

In the present study, the detailed effects of $(\text{H}_2\text{O})_n$ ($n = 1–3$) on the hydrogen atom transfer processes of the $\text{HO}_2 + \text{SO}_2 \rightarrow \text{HOSO} + {}^3\text{O}_2$ reaction have been investigated at the CCSD(T)/CBS//M06-2X/aug-cc-pVTZ level of theory, which is organized as follows. Firstly, incorporation of $(\text{H}_2\text{O})_n$ ($n = 1–3$) into the $\text{HO}_2 + \text{SO}_2 \rightarrow \text{HOSO} + \text{O}_2$ reaction produced two different types reactions: $\text{HO}_2 \cdots (\text{H}_2\text{O})_n$ ($n = 1–3$) + SO_2 and $\text{SO}_2 \cdots (\text{H}_2\text{O})_n$ ($n = 1–3$) + HO_2 . Then, these $(\text{H}_2\text{O})_n$ ($n = 1–3$)-catalyzed channels were evaluated by investigating the direct hydrogen abstraction process and the double hydrogen transfer mechanism. Secondly, the rate constants and effective rate constant of the hydrogen abstraction reaction of $\text{HO}_2 + \text{SO}_2 \rightarrow \text{HOSO} + \text{O}_2$ without and with $(\text{H}_2\text{O})_n$ ($n = 1–3$) were calculated to identify the favorable routes. Finally, the atmospheric relevance of the effect of $(\text{H}_2\text{O})_n$ ($n = 1–3$) was investigated by their competition with the primary loss mechanism of HO_2 radicals (such as the $\text{HO}_2 + \text{HO}_2$ and $\text{HO}_2 + \text{NO}_3$ reactions) and SO_2 (such as the $\text{SO}_2 + \text{HO}$ reaction). Overall, this work may lead to a better understanding of the effects of $(\text{H}_2\text{O})_n$ ($n = 1–3$) on gas-phase reactions under tropospheric conditions.

2. Computational details

The geometries of all the reactants, pre-reactive intermediates, post-reactive intermediates, transition states and products were optimized at the M06-2X/aug-cc-pVTZ level of theory,⁵⁵ and frequency analysis at the same level was performed to study the stationary point as well as the transition states. Moreover, the minimum energy path (MEP) was achieved by the intrinsic reaction coordinate (IRC)⁵⁶ theory with a gradient step size of $0.01–0.05 \text{ (amu)}^{1/2} \text{ Bohr}$, to confirm that the TS connects to minima along the reaction path. To obtain more reliable energy information, single-point energy calculations for the stationary points were obtained using the CCSD(T)⁵⁷/CBS method at the M06-2X/aug-cc-pVTZ optimized geometries. It is worth pointing out that single point energy calculations of CCSD(T)/CBS were carried out for all species at the CCSD(T) level of theory using the aug-cc-pVDZ and aug-cc-pVTZ basis sets. The energy values obtained at the DZ and TZ levels were used to extrapolate the results to a complete basis set (CBS) limit. The method used here for CBS extrapolation was proposed and developed by Varandas and Pansini.⁵⁸ In this method, the energy at the CBS limit is obtained by extrapolating the correlation (Corr) energy and Hartree–Fock (HF) energy separately using two different equations. To extrapolate the Corr energy and HF energy, the following equations were used:

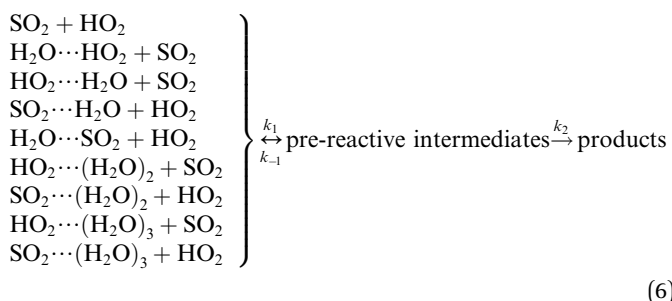
$$\text{CBS(Corr)} = \frac{2.71^3 E_{X+1} - 1.91^3 E_X}{2.71^3 - 1.91^3} \quad (4)$$

$$\text{CBS(HF)} = \frac{2.71^5 E_{X+1} - 1.91^5 E_X}{2.71^5 - 1.91^5} \quad (5)$$



To estimate the effect of $(\text{H}_2\text{O})_n$ ($n = 1-3$), the theoretical rate constants of canonical variational transition (CVT)⁵⁹⁻⁶¹ state theory with small curvature tunneling (SCT)^{62,63} correction for every reaction channel were calculated using the VKLab⁶⁴ program coupled with the steady state approximation.

As described in eqn (6), the $\text{HO}_2 + \text{SO}_2 \rightarrow \text{HOSO} + \text{O}_2$ reaction without and with $(\text{H}_2\text{O})_n$ ($n = 1-3$) all began with the formation of pre-reactive intermediates before occurring through the transition state.



Similar to the water-catalyzed $\text{OH} + \text{HOCl}$ reaction,²⁶ the free energy results displayed in Table S4[†] suggest that the intermediates are, in part, shifted to the reactants. Assuming that the pre-reactive intermediates of the $\text{HO}_2 + \text{SO}_2 \rightarrow \text{HOSO} + \text{O}_2$ reaction without and with $(\text{H}_2\text{O})_n$ ($n = 1-3$) are in equilibrium with the corresponding reactants and are at steady state, the overall rate constant of the $\text{SO}_2 + \text{HO}_2$ reaction is expressed as:

$$k = k_{\text{eq}} k_2 \quad (7)$$

$$k_{\text{eq}}(T) = \sigma \frac{Q_{\text{IM}}}{Q_{\text{R1}} Q_{\text{R2}}} \exp\left(\frac{E_{\text{R}} - E_{\text{IM}}}{RT}\right) \quad (8)$$

Here, the various Q values denote the partition functions of the intermediates, reactants R1 and R2. E_{R} and E_{IM} stand for the total energies of the reactants and intermediate, respectively, while σ is the symmetry factor. The rate constant k_2 of the second step of eqn (7) was evaluated by the VKLab⁶⁴ program in the framework of the CVT. To include tunneling effects for motion along the reaction coordinate of the title reaction at the CCSD(T)/CBS//M06-2X/aug-cc-pVTZ level, the SCT tunneling approximation was adopted. The electronic structure calculations were performed using Gaussian09 (ref. 65) software.

3. Results and discussion

The transition state in each reaction channel was denoted by "TS" followed by a number, and each pre-reactive intermediate was denoted by "IM" followed by a number. The letter "a" was used to distinguish the transition states and pre-reactive intermediates which are conformers of each other and therefore have the same features; species in the presence of H_2O , $(\text{H}_2\text{O})_2$, and $(\text{H}_2\text{O})_3$ were respectively denoted by a "WM", "WD", and "WT" suffix.

3.1 Potential energy surfaces for the $\text{SO}_2 + \text{HO}_2 \rightarrow \text{HOSO} + \text{O}_2$ reaction

Consistent with previous studies on the $\text{HO}_2 + \text{SO}_2$ reaction,^{3,11} three kinds of product pairs, $\text{HOSO} + \text{O}_2$, $\text{HSO}_2 + \text{O}_2$, and $\text{SO}_3 + \text{HO}$ could be found. Two H-abstraction channels and one O-abstraction route were modeled for the $\text{HO}_2 + \text{SO}_2$ reaction without water, as shown in Fig. S1.[†] From an energetic point of view, the channel for $\text{HOSO} + \text{O}_2$ formation was determined to be the major channel, and this is in good agreement with previous results reported by Wang *et al.*¹¹ Herein, as seen in Fig. 1, the $\text{SO}_2 + \text{HO}_2 \rightarrow \text{HOSO} + \text{O}_2$ reaction was mainly discussed, in order to focus on the catalytic role of $(\text{H}_2\text{O})_n$ ($n = 1-3$) in the $\text{SO}_2 + \text{HO}_2 \rightarrow \text{HOSO} + \text{O}_2$ reaction under atmospheric conditions. As shown in Fig. 1, for the formation of HOSO and O_2 , the reaction begins with the formation of the pre-reactive intermediate IM1. IM1 exhibits a five-membered ring structure. The relative energy of IM1 to the reactants ($\text{HO}_2 + \text{SO}_2$) is -5.6 kcal mol⁻¹, which is in reasonable agreement with the previous value (-6.2 kcal mol⁻¹) of CR1b reported by Wang *et al.*¹¹ The pre-reactive intermediate IM1 goes through an H-abstraction transition state TS1 to form the post-reactive intermediate IMF1. From an energetic standpoint, the transition state TS1 has been predicted to be 0.3 kcal mol⁻¹ below the reactants, which is slightly different from the corresponding values (-0.5 kcal mol⁻¹) obtained by Wang *et al.*¹¹ Intermediate IMF1 retains a five-membered ring structure with a binding energy of 1.4 kcal mol⁻¹, and it dissociates to produce $\text{HOSO} + \text{O}_2$, which lies 3.6 kcal mol⁻¹ above the energy of the $\text{HO}_2 + \text{SO}_2$ reactants.

3.2 Geometrical analysis of the $\text{HO}_2\cdots(\text{H}_2\text{O})_n$ ($n = 1-3$) and $\text{SO}_2\cdots(\text{H}_2\text{O})_n$ ($n = 1-3$) complexes

It is noteworthy that the rates of pure termolecular interactions are insignificant as compared to the rates of sequential bimolecular interactions.⁶⁷ In this sense, in the presence of $(\text{H}_2\text{O})_n$ ($n = 1-3$), both HO_2 and SO_2 mainly interact with $(\text{H}_2\text{O})_n$ ($n = 1-3$) *via* hydrogen bonding to form two-body complexes of $\text{HO}_2\cdots(\text{H}_2\text{O})_n$ ($n = 1-3$) and $\text{SO}_2\cdots(\text{H}_2\text{O})_n$ ($n = 1-3$), respectively, in the entrance channels, before interacting with the third body, SO_2 or HO_2 . Therefore, it is highly necessary to first find stable configurations of the complexes $\text{HO}_2\cdots(\text{H}_2\text{O})_n$ ($n = 1-3$) and $\text{SO}_2\cdots(\text{H}_2\text{O})_n$ ($n = 1-3$). In order to

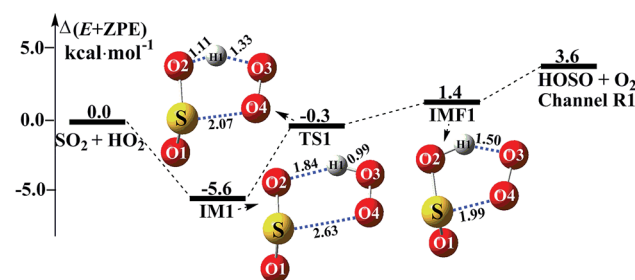


Fig. 1 Schematic energy diagrams of the $\text{SO}_2 + \text{HO}_2 \rightarrow \text{HOSO} + \text{O}_2$ reaction without water at the CCSD(T)/CBS//M06-2X/aug-cc-pVTZ level.



find all possible stable configurations of the complexes $\text{HO}_2\cdots(\text{H}_2\text{O})_n$ ($n = 1\text{--}3$) and $\text{SO}_2\cdots(\text{H}_2\text{O})_n$ ($n = 1\text{--}3$), global minimum searching of geometric structures was carried out using Tsinghua Global Minimum (TGMin).^{68,69} Then, the initial structures for $\text{HO}_2\cdots(\text{H}_2\text{O})_n$ ($n = 1\text{--}3$) and $\text{SO}_2\cdots(\text{H}_2\text{O})_n$ ($n = 1\text{--}3$) were selected for geometry optimization using the M06-2X/6-31G(d) method. The isomer structures within 6.0 kcal mol⁻¹ of the global minimum were re-optimized using the M06-2X/aug-cc-pVTZ method. Fig. 2 and S2† show the possible stable geometrical structures of $\text{HO}_2\cdots(\text{H}_2\text{O})_n$ ($n = 1\text{--}3$) and $\text{SO}_2\cdots(\text{H}_2\text{O})_n$ ($n = 1\text{--}3$), which are in good agreement with the available experimental results⁷⁰ and the previously calculated values.^{33,42,43,47} Interestingly, each type of equilibrium structure of the $\text{HO}_2\cdots(\text{H}_2\text{O})_n$ ($n = 1\text{--}3$) and $\text{SO}_2\cdots(\text{H}_2\text{O})_n$ ($n = 1\text{--}3$) complexes mainly differs in the relative orientations of the dangling hydrogen atoms of $(\text{H}_2\text{O})_n$ ($n = 1\text{--}3$). Thus, for each type of equilibrium structure of $\text{HO}_2\cdots(\text{H}_2\text{O})_n$ ($n = 1\text{--}3$) and $\text{SO}_2\cdots(\text{H}_2\text{O})_n$ ($n = 1\text{--}3$), as shown in Fig. 2, we focus our attention on only one configuration, which has a larger stabilization energy than its isomers.

As shown in Fig. 2, consistent with previous reports,^{70,71} the stable complex between HO_2 and H_2O is $\text{H}_2\text{O}\cdots\text{HO}_2$, which involves a five-membered ring structure. Its bonding energy, listed in Table S3,† is 6.9 kcal mol⁻¹, which is much more stable than hydrogen bonded (van der Waals interaction) complexes of $\text{HO}_2\cdots\text{H}_2\text{O}$, $\text{SO}_2\cdots\text{H}_2\text{O}$ and $\text{H}_2\text{O}\cdots\text{SO}_2$. Stable termolecular complexes of $\text{HO}_2\cdots(\text{H}_2\text{O})_2$ and $\text{SO}_2\cdots(\text{H}_2\text{O})_2$ are made up of HO_2 or SO_2 and a water dimer ($\text{H}_2\text{O}\cdots\text{H}_2\text{O}$). Similar to a binary complex of $\text{H}_2\text{O}\cdots\text{HO}_2$, both HO_2 (SO_2) and the water dimer in these two complexes act simultaneously as a hydrogen bond acceptor and a hydrogen bond donor. From an energetic standpoint, due to ring tension, the stabilization energy of the seven-membered-ring $\text{HO}_2\cdots(\text{H}_2\text{O})_2$ complex is 12.6 kcal mol⁻¹, whereas the

bonding energy of the six-membered ring $\text{SO}_2\cdots(\text{H}_2\text{O})_2$ complex is 6.9 kcal mol⁻¹. With HO_2 or SO_2 inserted into $(\text{H}_2\text{O})_3$, two stable geometries, $\text{HO}_2\cdots(\text{H}_2\text{O})_3$ and $\text{SO}_2\cdots(\text{H}_2\text{O})_3$, are obtained. Complex $\text{HO}_2\cdots(\text{H}_2\text{O})_3$ exhibits a nine-membered-ring structure with a bonding energy of 12.3 kcal mol⁻¹, which is less stable than that of complex $\text{HO}_2\cdots(\text{H}_2\text{O})_2$. Similarly, the binding energy of the eight-membered-ring $\text{SO}_2\cdots(\text{H}_2\text{O})_3$ complex is 6.5 kcal mol⁻¹, which is 0.4 kcal mol⁻¹ lower than that of $\text{SO}_2\cdots(\text{H}_2\text{O})_2$ due to the effect of ring strain. The present study mainly focuses on the catalytic roles of $(\text{H}_2\text{O})_n$ ($n = 1\text{--}3$) in the $\text{SO}_2 + \text{HO}_2 \rightarrow \text{HOSO} + \text{O}_2$ reaction. Only the favorable reaction channels will be discussed according to their energy barriers and thermodynamic properties. Details on the remaining reaction channels are presented in the ESI.†

3.3 Mechanism for H_2O -assisted $\text{SO}_2 + \text{HO}_2 \rightarrow \text{HOSO} + \text{O}_2$ reaction

The significance of the water-catalyzed $\text{SO}_2 + \text{HO}_2 \rightarrow \text{HOSO} + \text{O}_2$ reaction depends on the extent to which the respective bimolecular complexes, $\text{H}_2\text{O}\cdots\text{HO}_2$, $\text{HO}_2\cdots\text{H}_2\text{O}$, $\text{SO}_2\cdots\text{H}_2\text{O}$ and $\text{H}_2\text{O}\cdots\text{SO}_2$ exist, which can be determined by computing their stability, as above (Fig. 2), and their corresponding equilibrium constants, as shown in Table S2.† The equilibrium constants of these complexes at 298 K are 8.59×10^{-19} , 6.56×10^{-23} , 3.08×10^{-24} and 4.88×10^{-24} cm³ per molecule, respectively (Table S2†). Taking into account typical tropospheric concentrations of 7.73×10^{17} molecules per cm³ of H_2O , 3×10^8 molecules per cm³ of HO_2 ,⁷² and 1.0×10^{12} molecules per cm³ of SO_2 ,³³ it is estimated that the atmospheric concentration of the $\text{H}_2\text{O}\cdots\text{HO}_2$ complex is 1.99×10^8 molecules per cm³. Meanwhile, the concentrations of the $\text{HO}_2\cdots\text{H}_2\text{O}$, $\text{SO}_2\cdots\text{H}_2\text{O}$ and $\text{H}_2\text{O}\cdots\text{SO}_2$ complexes are estimated to be 1.52×10^4 , 2.38×10^6 , and 3.77×10^6 molecules per cm³. Thus, as shown in Fig. 3 and 4, when

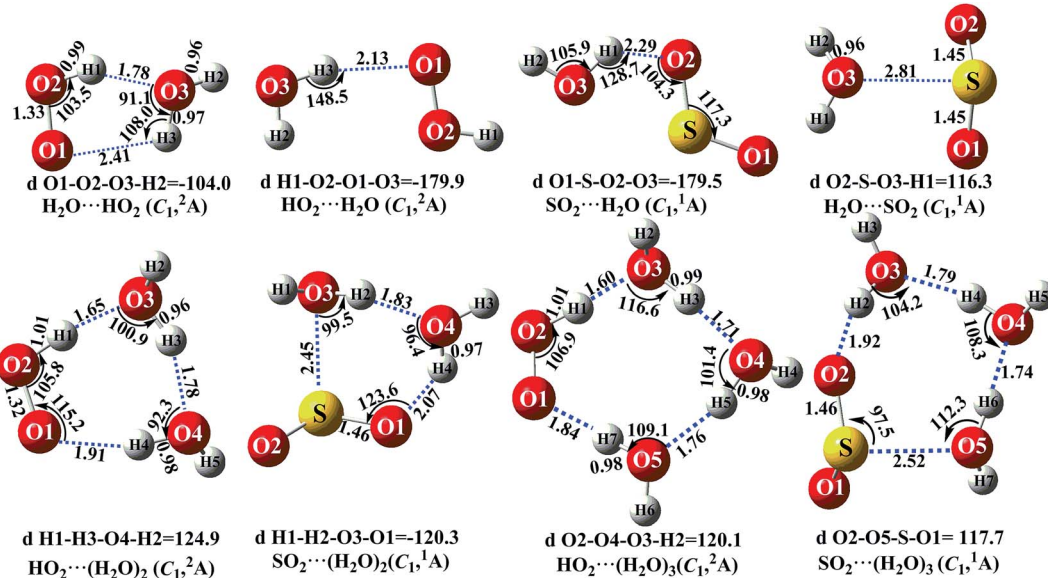


Fig. 2 The optimized geometrical reactants for the $\text{SO}_2 + \text{HO}_2$ reaction without and with catalyst X (X = H_2O , $(\text{H}_2\text{O})_2$ and $(\text{H}_2\text{O})_3$) at the M06-2X/aug-cc-pVTZ level of theory.

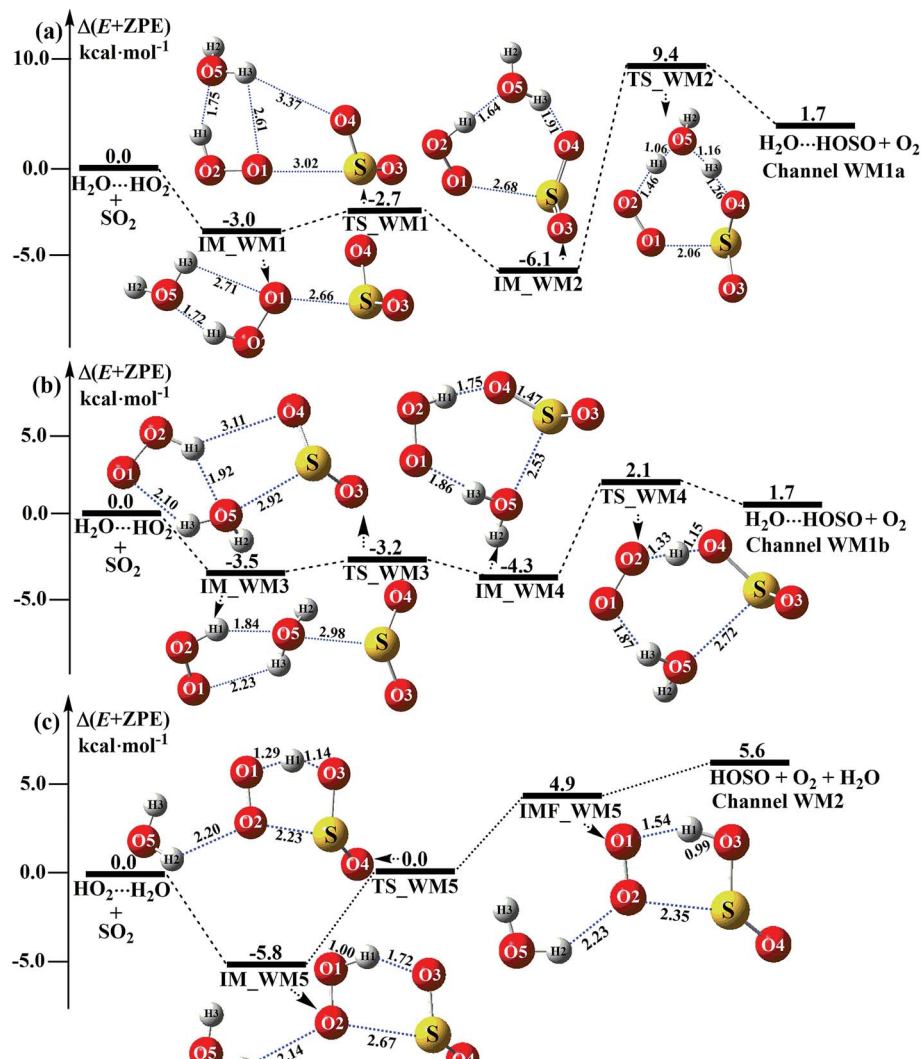
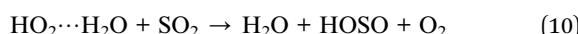


Fig. 3 Schematic energy diagrams of the water-assisted channel of $\text{HOSO} + \text{O}_2$ formation, occurring through $\text{H}_2\text{O}\cdots\text{HO}_2 + \text{SO}_2$ and $\text{HO}_2\cdots\text{H}_2\text{O} + \text{SO}_2$ at the CCSD(T)/CBS//M06-2X/aug-cc-pVTZ level.

one water molecule is introduced into the $\text{SO}_2 + \text{HO}_2 \rightarrow \text{HOSO} + \text{O}_2$ reaction, there are four possible types of bimolecular reactions, labeled as Channels WM1, WM2, WM3, and WM4.



3.3.1 Mechanism of $\text{H}_2\text{O}\cdots\text{HO}_2 + \text{SO}_2$ and $\text{HO}_2\cdots\text{H}_2\text{O} + \text{SO}_2$ reactions. For the formation of $\text{HOSO}\cdots\text{H}_2\text{O} + \text{O}_2$ occurring through the $\text{H}_2\text{O}\cdots\text{HO}_2 + \text{SO}_2$ reaction, Fig. 3 displays two Channels, namely Channel WM1a and Channel WM1b. Similar to other water-catalyzed reactions reported before,^{26,33,73} the influence of the water monomer in the $\text{H}_2\text{O}\cdots\text{HO}_2 + \text{SO}_2$

reaction was investigated by a stepwise mechanism, where the reaction occurs *via* a ring enlargement at first, and then proceeds through a hydrogen abstraction mechanism. However, the stepwise mechanism of Channel WM1a is different from Channel WM1b in three aspects. First, for the ring enlargement, the form of the $\text{S}\cdots\text{O}$ in complex IM_WM3 is different from that in complex IM_WM1. In complex IM_WM3, the $\text{S}\cdots\text{O}$ bond is formed by the S atom of SO_2 and the O atom of the H_2O moiety in the $\text{HO}_2\cdots\text{H}_2\text{O}$ complex, whereas the $\text{S}\cdots\text{O}$ bond in the IM_WM1 complex is formed by the S atom of SO_2 and the terminal O atom of the HO_2 moiety in the $\text{HO}_2\cdots\text{H}_2\text{O}$ complex. However, the stabilization energies of complexes IM_WM3 and IM_WM1 are close to each other, but with a difference of 0.5 kcal mol⁻¹. Secondly, the complex IM_WM4 has similar seven-membered cyclic structures as IM_WM2, except that SO_2 and H_2O have exchanged their positions. This is possibly the reason that the stabilization energy of complex IM_WM4 is 1.8 kcal mol⁻¹ lower than that of complex IM_WM2.

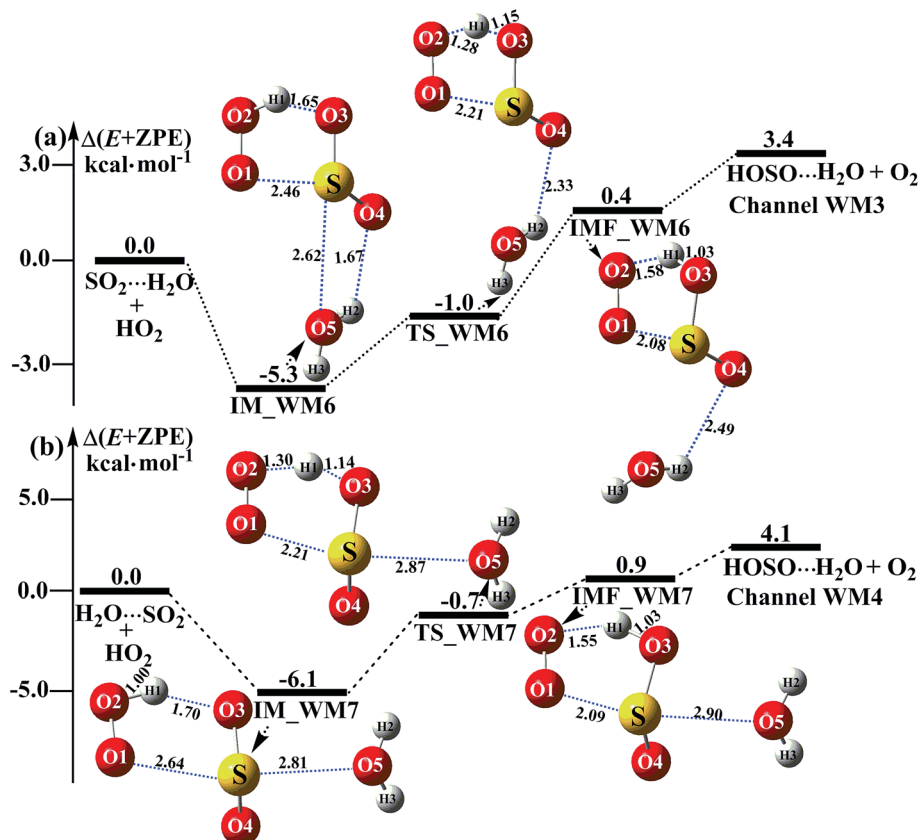


Fig. 4 Schematic energy diagrams of the water-assisted channel of HOSO + O₂ formation, occurring through SO₂···H₂O + HO₂ and H₂O···SO₂ + HO₂ at the CCSD(T)/CBS//M06-2X/aug-cc-pVTZ level.

The third one is that, for the rate-determining step of hydrogen abstraction, the barrier height of Channel WM1b is 2.1 kcal mol⁻¹, which is 7.3 kcal mol⁻¹ lower than the process of IM_WM2 → TS_WM2 → H₂O···HOSO + O₂ in Channel WM1a. This indicates that the double hydrogen transfer mechanism in Channel WM1a is less favorable than the direct hydrogen abstraction involved in Channel WM1b. This conclusion is consistent with our previous reports.^{71,73,74} As a result, in the following section, the reaction type of the multiple hydrogen transfer mechanism, where water molecules serve as a “bridge”, will be neglected in the stepwise reaction between SO₂ and HO₂···(H₂O)₂ (or HO₂···(H₂O)₃).

As for Channel WM2, it can be seen in Fig. 3c that a hydrogen bond complex, IM_WM5, has been identified, with a stabilization energy of 5.8 kcal mol⁻¹. From a geometrical point of view, complex IM_WM5 exhibits a five-membered ring structure, which is similar to the five-membered ring structure of complex IM1 in the reaction without a catalyst, as shown in Fig. 1. Compared with complex IM1, an additional O···H bond (O2···H2, 2.14 Å) is involved in IM_WM5. This leads to the stabilization energy of complex IM_WM5 being enhanced by 0.2 kcal mol⁻¹. Starting from complex IM_WM5 seen in Fig. 3c, the products HOSO + H₂O + O₂ can be obtained *via* transition state TS_WM5. From a geometrical point of view, similar to the naked transition state TS1, TS_WM5 follows direct hydrogen abstraction. Compared with TS1, the additional water molecule

in the transition state TS_WM5 is bonded to the terminal O atom of the HO₂ radical. Such a weak hydrogen bonding (O2···H2, 2.23 Å) interaction may lead to the energy of the TS_WM5 to HO₂···H₂O + SO₂ reactants being 0.3 kcal mol⁻¹ higher than that of the TS1 to the HO₂ + SO₂ reactants.

3.3.2 Potential energy surfaces for SO₂···H₂O + HO₂ and H₂O···SO₂ + HO₂ reactions. Beyond the water-assisted reaction channels described above, two additional water-assisted channels for HOSO + O₂ formation were found by taking into account the bimolecular reactions of SO₂···H₂O + HO₂ (Channel WM3) and H₂O···SO₂ + HO₂ (Channel WM4).

As for Channel WM3, the reaction of the SO₂···H₂O + HO₂ entry channel proceeds through the formation of complex IM_WM6 before the transition state TS_WM6 and complex IMF_WM6. From a geometric point of view, complex IM_WM6 has one five-membered ring, H(1)–O(2)–O(1)···S–O(3), and one four-membered ring, O(4)···H(2)–O(5)···S, with a computed relative energy of 5.3 kcal mol⁻¹ below the reactants of SO₂···H₂O + HO₂, as shown in Table S4† and Fig. 4. Starting from complex IM_WM6, with the H atom of HO₂ migrating to one O atom of the SO₂ moiety in the SO₂···H₂O complex, the reaction can proceed *via* the transition state TS_WM6 to form complex IMF_WM6. As shown in Fig. 4, only the five-membered ring was retained in both the transition state TS_WM6 and complex IMF_WM6 with the elongation of the S···O5 bond. Compared with the transition state TS1 in Fig. 1, the additional water

molecule in TS_WM6 did not change the active features of the five-membered ring. Furthermore, with the water molecule added, the relative energy of TS_WM6 to $\text{SO}_2\cdots\text{H}_2\text{O} + \text{HO}_2$ is 0.7 kcal mol⁻¹ less than the corresponding value of TS1 (-0.3 kcal mol⁻¹) to $\text{SO}_2 + \text{HO}_2$.

The fourth channel of the water-assisted $\text{SO}_2 + \text{HO}_2 \rightarrow \text{HOSO} + \text{O}_2$ reaction (Channel WM4, Fig. 4b) begins with complex IM_WM7 *via* the interaction between the O atom of H_2O and the S atom of the SO_2 moiety in $\text{H}_2\text{O}\cdots\text{SO}_2$. The relative energy of complex IM_WM7 to the $\text{H}_2\text{O}\cdots\text{SO}_2 + \text{HO}_2$ reactants is 6.1 kcal mol⁻¹. Complex IM_WM7 then decomposes *via* transition state TS_WM7 to form complex IMF_WM7. As shown in Fig. 4, similar to the structure of TS_WM6 and complex IMF_WM6, a five-membered ring is still involved in both TS_WM7 and complex IMF_WM7. Compared with TS1 in Fig. 1, the additional water molecule in TS_WM7 leads to the relative energy of TS_WM7 to $\text{H}_2\text{O}\cdots\text{SO}_2 + \text{HO}_2$ being 0.7 kcal mol⁻¹, which is 0.4 kcal mol⁻¹ less than the corresponding value of TS1 (-0.3 kcal mol⁻¹) to $\text{SO}_2 + \text{HO}_2$.

3.4 Mechanism for $(\text{H}_2\text{O})_2$ -catalyzed the $\text{SO}_2 + \text{HO}_2 \rightarrow \text{HOSO} + \text{O}_2$ reaction

As shown in Fig. 5, $(\text{H}_2\text{O})_2$ catalyzed channels were determined, starting from $\text{HO}_2\cdots(\text{H}_2\text{O})_2 + \text{SO}_2$ and $\text{SO}_2\cdots(\text{H}_2\text{O})_2 + \text{HO}_2$ reactants, which are labeled as Channel WD1 and Channel WD2.

For the $\text{HO}_2\cdots(\text{H}_2\text{O})_2 + \text{SO}_2$ reaction (Channel WD1), two reaction types, namely Channel WD1a and Channel WD1b were found, depending on how the S atom of SO_2 approaches the complex of $\text{HO}_2\cdots(\text{H}_2\text{O})_2$. In the same way as the $\text{H}_2\text{O}\cdots\text{HO}_2 + \text{SO}_2$ reaction above (Fig. 3), both Channels WD1a and WD1b occur *via* a stepwise mechanism, which involves a direct hydrogen abstraction with one O atom of SO_2 abstracting the H atom of a HO_2 moiety in the $\text{HO}_2\cdots(\text{H}_2\text{O})_2$ complex. However, as shown in Fig. 5, unlike the hydrogen abstraction in Channel WD1a, where the number of rings increases with decreasing ring size, in Channel WD1b the hydrogen abstraction does not change the ring size or the ring number. This discrepancy of hydrogen abstraction between Channels WD1a and WD1b may mean that, in Channel WD1a, the barrier height of the rate determining step ($\text{IM}_\text{WD2} \rightarrow \text{TS}_\text{WD2} \rightarrow (\text{H}_2\text{O})_2\cdots\text{HOSO} + \text{O}_2$) is 8.4 kcal mol⁻¹ higher than the corresponding barrier height of the rate determining step ($\text{IM}_\text{WD4} \rightarrow \text{TS}_\text{WD4} \rightarrow (\text{H}_2\text{O})_2\cdots\text{HOSO} + \text{O}_2$) in Channel WD1b. As a result, for the $\text{HO}_2\cdots(\text{H}_2\text{O})_2 + \text{SO}_2$ reaction, Channel WD1b is mainly taken into account here.

For Channel WD1b, with the interaction between the S atom of SO_2 and O(5) of the H_2O moiety in the $\text{HO}_2\cdots(\text{H}_2\text{O})_2$ complex, the reaction begins with the seven-membered cyclic complex IM_WD3, whose stability has been computed to be 2.7 kcal mol⁻¹. Then, the reaction proceeds through the ring enlargement from IM_WD3 to IM_WD4 *via* the transition state TS_WD3, with an energy barrier of 1.5 kcal mol⁻¹. Complex IM_WD4 has a similar structure to IM_WM4 (Fig. 3), but with a water monomer substituted by a water dimer. The binding energy of IM_WD4 is 1.8 kcal mol⁻¹, which is 0.9 kcal mol⁻¹ less

stable than the complex IM_WD3. Starting from the complex IM_WD4, the reaction can proceed *via* the transition state TS_WD4 to form the products of $(\text{H}_2\text{O})_2\cdots\text{HOSO} + \text{O}_2$. Similar to complex IM_WD4, TS_WD4 also shows a nine-membered ring structure with three components of $(\text{H}_2\text{O})_2$, the SO moiety of SO_2 and the HO_2 radical. The relative energy of TS_WD4 to $\text{HO}_2\cdots(\text{H}_2\text{O})_2 + \text{SO}_2$ is 0.4 kcal mol⁻¹, which is 2.5 kcal mol⁻¹ lower than that of the H_2O -assisted transition state TS_WM4 to $\text{H}_2\text{O}\cdots\text{HO}_2 + \text{SO}_2$ reactants. Meanwhile, from the viewpoint of ring sizes, for TSW2 and TSWD, with the ring size increase, the rate constant of the rate-determining step increases when one water molecule has been replaced by a water dimer. This is possibly because when the seven-membered ring has been replaced by a nine-membered ring, the number of hydrogen bonds increases, leading to the stabilization of the ring increasing. These facts indicate that the second water molecule plays a positive catalytic role by significantly reducing the barrier height of the $\text{SO}_2 + \text{HO}_2 \rightarrow \text{HOSO} + \text{O}_2$ reaction.

As for Channel WD2, starting from $\text{SO}_2\cdots(\text{H}_2\text{O})_2 + \text{HO}_2$ reactants, the reaction begins with the formation of complex IM_WD5. As shown in Fig. 5c, complex IM_WD5 exhibits a double-ring structure with a five-membered ring, $\text{O}_2\cdots\text{H}_1\cdots\text{O}_3\cdots\text{S}\cdots\text{O}_1$, and a six-membered ring, $\text{O}_4\cdots\text{H}_2\cdots\text{O}_5\cdots\text{H}_4\cdots\text{O}_6\cdots\text{S}$. Aside from these characteristics, complex IM_WD5 has a similar structure to that of IM_WM5, but with an additional water molecule inserted at the site between H_2O and SO_2 . This leads to the stabilization energy of complex IM_WD5 (Table S4† and Fig. 5) being enhanced by 0.3 kcal mol⁻¹ compared with complex IM_WM5. After complex IM_WD5, with the H atom of HO_2 migrating to one O atom of the SO_2 moiety in the $\text{SO}_2\cdots(\text{H}_2\text{O})_2$ complex, the products of $\text{HOSO}\cdots(\text{H}_2\text{O})_2 + \text{O}_2$ can be obtained *via* transition state TS_WD5 and complex IMF_WD5. As shown in Fig. 5, the double-ring structure is retained in transition state TS_WD5 and complex IMF_WD5. Compared with TS_WM5 in Fig. 4, with the introduction of the second water molecule, the active features of the five-membered ring in TS_WD5 exhibit no change. The relative energy of TS_WD5 to $\text{SO}_2\cdots(\text{H}_2\text{O})_2 + \text{HO}_2$ is 0.9 kcal mol⁻¹, which is only changed by 0.6–0.9 kcal mol⁻¹ compared with the corresponding values of TS_WM5 with H_2O and TS1 without a catalyst. This implies that Channel WD2 proceeds easily.

3.5 Mechanism for $(\text{H}_2\text{O})_3$ -catalyzed the $\text{SO}_2 + \text{HO}_2 \rightarrow \text{HOSO} + \text{O}_2$ reaction

Similar to the instance of the $(\text{H}_2\text{O})_2$ -assisted reaction that occurs through the $\text{HO}_2\cdots(\text{H}_2\text{O})_2 + \text{SO}_2$ and $\text{SO}_2\cdots(\text{H}_2\text{O})_2 + \text{HO}_2$ reactions discussed above, the $(\text{H}_2\text{O})_3$ -assisted $\text{SO}_2 + \text{HO}_2 \rightarrow \text{HOSO} + \text{O}_2$ reaction can be obtained both by the insertion of SO_2 into the $\text{HO}_2\cdots(\text{H}_2\text{O})_3$ complex, and by the collision of the HO_2 radical with the $\text{SO}_2\cdots(\text{H}_2\text{O})_3$ complex. Through the $\text{SO}_2\cdots(\text{H}_2\text{O})_3 + \text{HO}_2$ reaction (which proceeds easily, as shown in Table S6,† with an energy barrier of 1.3 kcal mol⁻¹, as shown in Table S2†), the concentration of $\text{SO}_2\cdots(\text{H}_2\text{O})_3$ at 298 K is 4 orders of magnitude smaller than that of $\text{HO}_2\cdots(\text{H}_2\text{O})_3$. Therefore, the $\text{SO}_2\cdots(\text{H}_2\text{O})_3 + \text{HO}_2$ reaction can be neglected under tropospheric conditions, and herein, we only focus our attention on



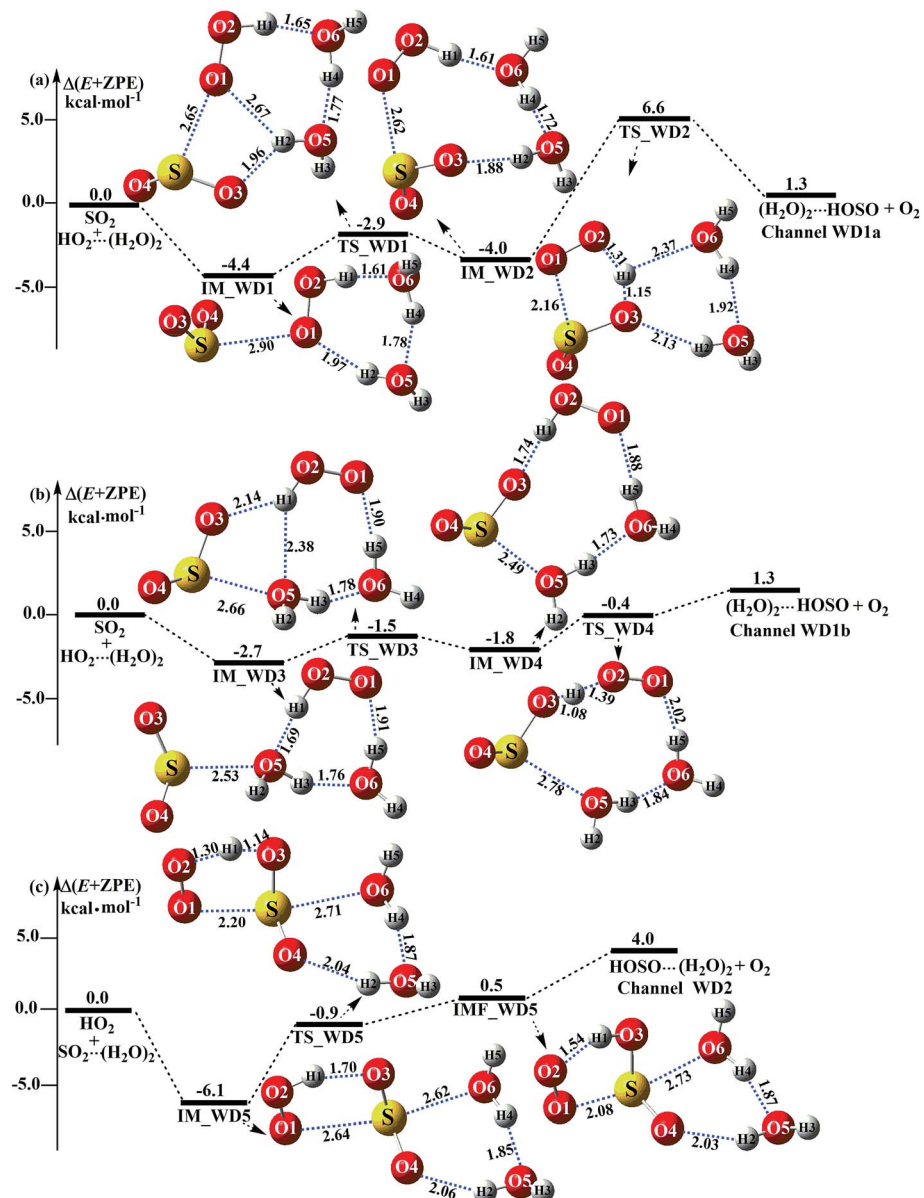


Fig. 5 Schematic energy diagrams of the dimer water-assisted channel of $\text{HOSO} + \text{O}_2$ formation, occurring through $\text{HO}_2\cdots(\text{H}_2\text{O})_2 + \text{SO}_2$ and $\text{SO}_2\cdots(\text{H}_2\text{O})_2 + \text{HO}_2$ at the CCSD(T)/CBS//M06-2X/aug-cc-pVTZ level.

the $\text{HO}_2\cdots(\text{H}_2\text{O})_3 + \text{SO}_2$ reaction. For comparison, a schematic energy diagram of $\text{HO}_2 + \text{SO}_2\cdots(\text{H}_2\text{O})_3$ reaction is displayed in Fig. S6.†

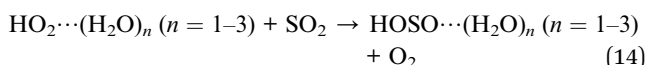
Similar to $\text{H}_2\text{O}\cdots\text{HO}_2 + \text{SO}_2$ and $\text{HO}_2\cdots(\text{H}_2\text{O})_2 + \text{SO}_2$ reactions above, $\text{HO}_2\cdots(\text{H}_2\text{O})_2 + \text{SO}_2$ reaction (Channel WT1) shown in Fig. 6 also proceeds through a stepwise mechanism to form $\text{HOSO}\cdots(\text{H}_2\text{O})_3 + \text{O}_2$. In the first step, the reaction starts with complex IM_WT1, which has a binding energy of 3.0 kcal mol⁻¹. From a geometrical point of view, complex IM_WT1 has one nine-membered ring-like structure. After complex IM_WT1, the ring enlargement from complex IM_WT1 to the eleven-membered ring complex IM_WT2 occurs *via* the double-ring transition state TS_WT1 (nine-membered ring, right; four-membered ring, left) with a barrier height of 0.7 kcal mol⁻¹.

Complex IM_WT2 has similar quasi-planar structures to IM_WD4, with an additional water molecule inserted between SO_2 and HO_2 . Complex IM_WT2 is 1.0 kcal mol⁻¹ less stable than IM_WT1, and is also 0.8 kcal mol⁻¹ less stable than IM_WD4. In the second step, following complex IM_WT2, Channel WT1 proceeds through transition state TS_WT2 to produce the product of $\text{HOSO}\cdots(\text{H}_2\text{O})_3 + \text{O}_2$. At transition state TS_WT2, the eleven-membered ring structure is still conserved, and the structure is similar to TS_WD4, but with an additional water molecule inserted between SO_2 and HO_2 . From the viewpoint of ring sizes, for TS_WT2 and TS_WD4, although the hydrogen bonds increase in the ring when the nine-membered ring becomes an eleven-membered ring, the eleven-membered ring is unstable, and the tension is large, so TS_WT2 lies

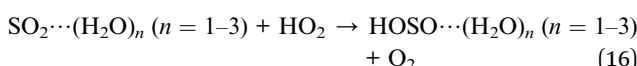
16.0 kcal mol⁻¹ above the HO₂···(H₂O)₃ + SO₂ reactants, which is 16.4 kcal mol⁻¹ higher in energy than the relative energy of TS_WD4 to HO₂···(H₂O)₂ + SO₂ reactants. Meanwhile, the rate constant of the rate-determining step decreases when the water dimer has been replaced by the water trimer (Fig. 6).

3.6 Reaction kinetics

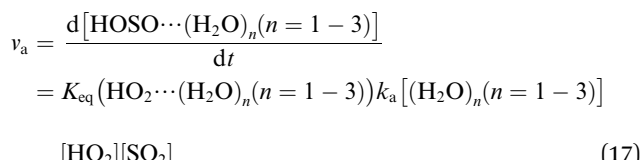
With regard to the reactions involving $(\text{H}_2\text{O})_n$ ($n = 1-3$), we consider $\text{HO}_2 \cdots (\text{H}_2\text{O})_n$ ($n = 1-3$) and SO_2 or $\text{SO}_2 \cdots (\text{H}_2\text{O})_n$ ($n = 1-3$) and HO_2 . When $\text{HO}_2 \cdots (\text{H}_2\text{O})_n$ ($n = 1-3$) and SO_2 act as reactants, the reactions occur *via* the following reaction mechanism:



Meanwhile when $\text{SO}_2 \cdots (\text{H}_2\text{O})_n$ ($n = 1\text{--}3$) and HO_2 are considered to be the reactants, the reaction mechanism is as follows:



The rate *via* the reaction processes (13) and (14) is expressed in eqn (17).



Here, $K_{\text{eq}}(\text{HO}_2 \cdots (\text{H}_2\text{O})_n \ (n = 1-3))$ is the equilibrium constant for the formation of the $\text{HO}_2 \cdots (\text{H}_2\text{O})_n \ (n = 1-3)$ complex from isolated HO_2 and $(\text{H}_2\text{O})_n \ (n = 1-3)$ and k_r represents the rate

constant of eqn (14). The rate *via* the reaction processes (15) and (16) is expressed in eqn (18).

$$v_b = \frac{d[HOSO \cdots (H_2O)_n (n=1-3)]}{dt} \\ = K_{eq}(SO_2 \cdots (H_2O)_n (n=1-3)) k_b [(H_2O)_n \\ (n=1-3)][HO_2][SO_2] \quad (18)$$

Here, $K_{\text{eq}}(\text{SO}_2 \cdots (\text{H}_2\text{O})_n \ (n = 1-3))$ is the equilibrium constant for the formation of the $\text{SO}_2 \cdots (\text{H}_2\text{O})_n \ (n = 1-3)$ complex from isolated SO_2 and $(\text{H}_2\text{O})_n \ (n = 1-3)$ and k_b represents the rate constant of eqn (16). It is worth noting that, herein, we do not consider how pressure effects influence the formation of these complexes, because there are no experimental results showing that the equilibrium constants of these complexes depend on pressure.

The computed rate constants are provided in Table 1. For the reaction without a catalyst, the computed rate constant ($k_{(R1)}$) is 9.09×10^{-18} to 5.22×10^{-17} cm³ per molecule per s in the temperature range of 218.6–320.0 K. At 298 K, the calculated value of $k_{(R1)}$ is 3.87×10^{-17} cm³ per molecule per s, which is close to the experimental value (1.0×10^{-18} cm³ per molecule per s).⁶⁶ For the reaction with (H₂O)_n ($n = 1$ –3), the rate ratio v_a/v_b of the HO₂ + SO₂ + (H₂O)_n ($n = 1$ –3) reaction shows that the entrance of HO₂···(H₂O)_n ($n = 1$ –3) and SO₂ is more important than that of SO₂···(H₂O)_n ($n = 1$ –3) and HO₂ because the rate ratios v_{a1}/v_{b1} , v_{a2}/v_{b2} , and v_{a3}/v_{b3} are 2.15×10^9 to 1.27×10^7 , 5.00×10^8 to 4.95×10^6 , 4.03×10^{13} to 4.12×10^9 , respectively, between 275.0 and 320.0 K (Table 1).

In the $\text{HO}_2\cdots(\text{H}_2\text{O})_n$ ($n = 1-3$) + SO_2 reaction, it is necessary to calculate its effective rate constant k' , which can be considered as a measure of the efficiencies of the different catalysts of $(\text{H}_2\text{O})_n$ ($n = 1-3$) under atmospheric conditions, as it includes the concentration of $(\text{H}_2\text{O})_n$ ($n = 1-3$), equilibrium constants of $\text{HO}_2\cdots(\text{H}_2\text{O})_n$ ($n = 1-3$), and the rate constant from eqn (14). Based on this, the rates for the channels of the $\text{H}_2\text{O}\cdots\text{HO}_2 + \text{SO}_2$ reaction (k_{WM1b}), the

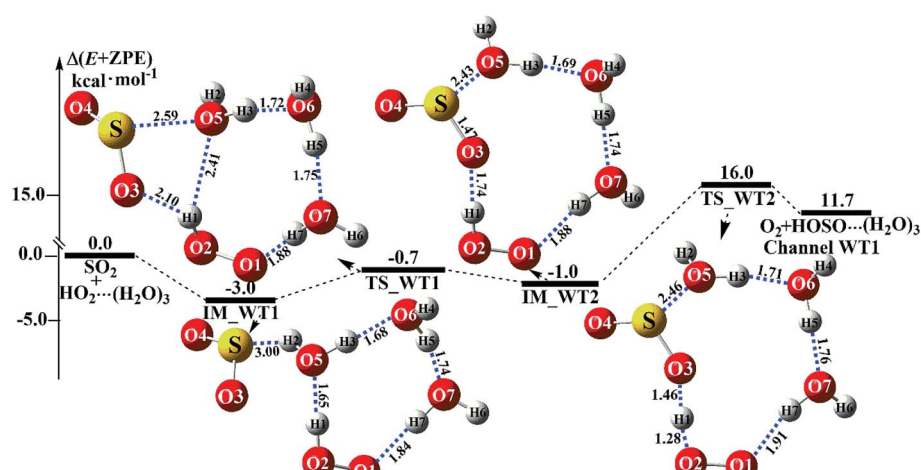


Fig. 6 Schematic energy diagrams of the trimer water-assisted channel of $\text{HOSO} + \text{O}_2$ formation, occurring through $\text{HO}_2 \cdots (\text{H}_2\text{O})_3 + \text{SO}_2$ at the CCSD(T)/CBS/M06-2X/aug-cc-pVTZ level

Table 1 Ratio of reaction rate and effective rate constants (cm³ per molecules per s) for HOSO + O₂ formation from the SO₂ + HO₂ reaction without and with (H₂O)_n (*n* = 1–3) within the temperature range of 275.0–320.0 K^a

T (K)	<i>k</i> _R	<i>v</i> _{a1} / <i>v</i> _{b1}	<i>v</i> _{a2} / <i>v</i> _{b2}	<i>v</i> _{a3} / <i>v</i> _{b3}	<i>k'</i> _a (WM1)	<i>k'</i> _a (WD1)	<i>k'</i> _a (WT1)
218.6	9.09×10^{-18}	2.15×10^9	5.00×10^8	4.03×10^{13}	5.84×10^{-13}	2.99×10^{-23}	—
223.7	1.02×10^{-17}	1.48×10^9	3.69×10^8	1.73×10^{14}	5.38×10^{-13}	3.57×10^{-22}	—
229.7	1.08×10^{-17}	9.78×10^7	3.96×10^8	1.78×10^{12}	4.93×10^{-13}	5.07×10^{-18}	1.68×10^{-21}
235.1	1.31×10^{-17}	6.82×10^8	1.97×10^8	9.96×10^{11}	4.57×10^{-13}	1.81×10^{-18}	—
249.9	1.75×10^{-17}	2.78×10^9	9.59×10^7	1.58×10^{12}	3.83×10^{-13}	5.73×10^{-18}	—
259.3	1.76×10^{-17}	1.66×10^8	4.07×10^5	3.24×10^{11}	3.47×10^{-13}	3.09×10^{-18}	5.95×10^{-21}
275.0	2.72×10^{-17}	7.64×10^7	3.47×10^7	8.65×10^{10}	3.02×10^{-13}	3.90×10^{-17}	1.63×10^{-19}
280.0	2.95×10^{-17}	6.07×10^7	2.92×10^7	3.10×10^{10}	2.90×10^{-13}	4.57×10^{-17}	1.55×10^{-18}
290.0	3.44×10^{-17}	3.92×10^7	2.09×10^7	4.12×10^9	2.71×10^{-13}	6.58×10^{-17}	1.54×10^{-19}
298.2	3.87×10^{-17}	2.82×10^8	1.63×10^8	7.88×10^{13}	2.57×10^{-13}	8.95×10^{-17}	1.59×10^{-18}
300.0	3.98×10^{-17}	2.62×10^8	1.54×10^7	3.19×10^{13}	2.54×10^{-13}	9.50×10^{-17}	1.58×10^{-18}
310.0	4.57×10^{-17}	1.80×10^8	1.16×10^7	4.87×10^{10}	2.41×10^{-13}	1.32×10^{-16}	1.57×10^{-19}
320.0	5.22×10^{-17}	1.27×10^7	4.95×10^6	2.72×10^{11}	2.30×10^{-13}	1.72×10^{-16}	1.48×10^{-18}

^a The letters “a” and “b” are used to distinguish the complexes: “a” is the complex of HO₂···(H₂O)_n (*n* = 1–3), while “b” is the complex of SO₂···(H₂O)_n (*n* = 1–3). *v*_{a1}, *v*_{a2} and *v*_{a3} are the reaction rates of HO₂···(H₂O)_n (*n* = 1–3), *v*_{b1}, *v*_{b2} and *v*_{b3} are the equilibrium constants of SO₂···(H₂O)_n (*n* = 1–3). Species in the presence of a water molecule, water dimer and water trimer are respectively denoted by “1”, “2”, and “3”. *k'*_a(WM1) is the effective rate constant for the process of HO₂···H₂O + SO₂ → HOSO···H₂O + O₂. *k'*_a(WD1) is the rate constant for the process of HO₂···(H₂O)₂ + SO₂ → HOSO···(H₂O)₂ + O₂. *k'*_a(WT1) is the rate constant for the process of HO₂···(H₂O)₃ + SO₂ → HOSO···(H₂O)₃ + O₂.

HO₂···(H₂O)₂ + SO₂ reaction (*k*_a(WD1b)) and the HO₂···(H₂O)₃ + SO₂ reaction (*k*_a(WT1)) are respectively written as follows.

$$\begin{aligned} v_a(\text{WM1b}) &= k_a(\text{WM1b})[\text{H}_2\text{O} \cdots \text{HO}_2][\text{SO}_2] \\ &= k'_a(\text{WM1b})[\text{SO}_2][\text{HO}_2] \end{aligned} \quad (19)$$

$$\begin{aligned} v_a(\text{WD1b}) &= k_a(\text{WD1b})[\text{HO}_2 \cdots (\text{H}_2\text{O})_2][\text{SO}_2] \\ &= k'_a(\text{WD1b})[\text{HO}_2][\text{SO}_2] \end{aligned} \quad (20)$$

$$\begin{aligned} v_a(\text{WT1}) &= k_a(\text{WT1})[\text{HO}_2 \cdots (\text{H}_2\text{O})_3][\text{SO}_2] \\ &= k'_a(\text{WT1})[\text{HO}_2][\text{SO}_2] \end{aligned} \quad (21)$$

In these equations, *k'*_a(WM1b) = *k*_a(WM1b)*K*_{eq}(H₂O···HO₂)[H₂O]; *k'*_a(WD1b) = *k*_a(WD1b)*K*_{eq}(HO₂···(H₂O)₂)[(H₂O)₂]; and *k'*_a(WT1) = *k*_a(WT1)*K*_{eq}(HO₂···(H₂O)₃)[(H₂O)₃]. *K*_{eq}(H₂O···HO₂), *K*_{eq}(HO₂···(H₂O)₂) and *K*_{eq}(HO₂···(H₂O)₃) are the equilibrium constants for the formation of the H₂O···HO₂, HO₂···(H₂O)₂ and HO₂···(H₂O)₃ complexes, respectively. [H₂O], [(H₂O)₂] and [(H₂O)₃] are the concentrations of H₂O, (H₂O)₂, and (H₂O)₃, respectively. As shown in Table 1, within the temperature range of 275.0–320.0 K, the effective rate constant of *k'*_a(WM1b) is 1.32×10^{-14} to 2.01×10^{-14} cm³ per molecule per s, which is 2–3 and 3–6 orders of magnitude larger than the corresponding values of *k'*_a(WD1b) and *k'*_a(WT1), respectively, indicating that the catalytic effect of H₂O is the largest among the (H₂O)_n (*n* = 1–3) catalysts, and the catalytic effect of (H₂O)₂, and (H₂O)₃ is negligible. Compared with the rate constant of the naked reaction of SO₂ + HO₂ → HOSO + O₂, the value of *k'*_a(WM1b) is 2–3 orders of magnitude larger within the temperature range of 275.0–320.0 K, indicating that at 0 km altitude within this temperature range, the positive effect of water is significant under atmospheric conditions.

The average concentrations of water at 5, 10 and 15 km altitudes are known to be 2.41×10^{16} , 4.92×10^{15} and 1.96×10^{13} molecules per cm³, respectively.⁷⁵ Considering the average concentrations of water at 5, 10 and 15 km altitudes in the troposphere, the calculated effective rate constants of the H₂O-

assisted Channel WM1, the (H₂O)₂-assisted Channel WD1 and the (H₂O)₃-assisted Channel WT1 are listed in Table 2. Compared with an altitude of 0 km, the dominant channel does not change in the three different cases, which is similar to the dominant channel in Table 1. Meanwhile, the values of *k'*(WM1) are 7.49×10^{-17} , 2.68×10^{-17} and 2.95×10^{-18} at altitudes of 5, 10 and 15 km, respectively. Compared with the value of *k'*(WM1) at 0 km, we found that the values of *k'*(WM1) show a declining trend, decreasing by about 4–5 orders of magnitude, as we move towards higher altitude. Furthermore, as shown in Table 2, it has been estimated that the enhancement factors of water vapor are 99.98%, 78.23%, 69.63% and 27.27% at altitudes of 0, 5, 10 and 15 km, respectively. This implies that, as we move towards higher altitudes, the contribution of water on increasing the reaction rate becomes gradually lessened.

3.7 Atmospheric implications

In gas-phase reactions of the atmosphere, previous investigations have shown that the dominant sink of HO₂ is its reaction with HO₂ (ref. 71) and NO₃.⁷⁶ Therefore, it is of great importance to discuss the effective rate constant of the H₂O···HO₂ + SO₂ reaction (*k'*_a(WM1b)) with the rate constant of these dominant sink processes of HO₂. To meet this goal, the reaction mechanisms of HO₂ + HO₂ and HO₂ + NO₃ at the CCSD(T)/CBS//M06-2X/aug-cc-pVTZ level are shown in Fig. S7,[†] while their rate constants within the temperature range of 218.6–320.0 K are listed in Table 3, with rate ratios between H₂O···HO₂ + SO₂ and HO₂ + HO₂ (HO₂ + NO₃) as shown in eqn (22). The calculated rate constants are in good agreement with the available experimental values.^{77–79}

$$\begin{aligned} \frac{v_{a1}}{v_{R1}} &= \frac{K_{eq}(\text{H}_2\text{O} \cdots \text{HO}_2)k_a(\text{WM1b})[\text{H}_2\text{O}][\text{HO}_2][\text{SO}_2]}{k_{R1}[\text{HO}_2][\text{HO}_2]} \\ &= \frac{K_{eq}(\text{H}_2\text{O} \cdots \text{HO}_2)k_a(\text{WM1b})[\text{H}_2\text{O}][\text{SO}_2]}{k_{R1}[\text{HO}_2]} \end{aligned} \quad (22)$$



Table 2 Effective rate constants (cm³ per molecules per s) for HOSO + O₂ formation from the SO₂ + HO₂ reaction without and with (H₂O)_n (*n* = 1–3) within the altitude range of 0–15 km^a

Alt. (km)	T (K)	<i>k'</i> _a (WM1)	<i>k'</i> _a (WD1)	<i>k'</i> _b (WD2)	<i>k'</i> _a (WT1)	<i>k'</i> _a (WM)/ <i>k</i> _{tot}
0	298.2	1.67 × 10 ⁻¹³	1.15 × 10 ⁻²¹	4.03 × 10 ⁻¹⁷	1.59 × 10 ⁻¹⁸	99.98%
5	259.3	7.49 × 10 ⁻¹⁷	3.09 × 10 ⁻¹⁸	1.10 × 10 ⁻¹⁸	3.53 × 10 ⁻²⁰	78.23%
10	229.7	2.68 × 10 ⁻¹⁷	5.07 × 10 ⁻¹⁸	1.40 × 10 ⁻¹⁸	1.68 × 10 ⁻²¹	69.63%
15	212.6	2.95 × 10 ⁻¹⁸	8.95 × 10 ⁻¹⁷	2.63 × 10 ⁻²²	2.42 × 10 ⁻²⁶	27.27%

^a *k'*_a(WM1) is the effective rate constant occurring through Channel WM1. *k'*_a(WD1) and *k'*_b(WD2) are the effective rate constants of Channel WD1 and WD2, respectively; *k'*_a(WT1) is the effective rate constant of Channel WT1. *k*_{tot} = *k*_{R1} + *k'*_a(WM)(100% RH).

$$\begin{aligned} \frac{v_{a1}}{v_{R2}} &= \frac{K_{eq}(\text{H}_2\text{O} \cdots \text{HO}_2)k_a(\text{WM1b})[\text{H}_2\text{O}][\text{HO}_2][\text{SO}_2]}{k_{R2}[\text{HO}_2][\text{NO}_3]} \\ &= \frac{K_{eq}(\text{H}_2\text{O} \cdots \text{HO}_2)k_a(\text{WM1b})[\text{H}_2\text{O}][\text{SO}_2]}{k_{R2}[\text{NO}_3]} \end{aligned} \quad (23)$$

Here, *k*_{R1} and *k*_{R2} are the rate constants of the HO₂ + HO₂ reaction and the HO₂ + NO₃ reaction, respectively, obtained from Table 3. The rate ratios *v*_{a1}/*v*_{R1} and *v*_{a1}/*v*_{R2} depend on the H₂O, SO₂, NO₃ and HO₂ concentrations in the atmosphere. At 298 K, when the concentration of water is at a relative humidity of 100%, SO₂ and NO₃ are 7.73 × 10¹⁷, 1 × 10¹² and 2.46 × 10⁷ molecules per cm³, respectively, and the gas-phase concentration of HO₂ is 3 × 10⁸ molecules per cm³, the H₂O · · HO₂ + SO₂ reaction can compete with the HO₂ + HO₂ reaction, because the rate ratio *v*_{a1}/*v*_{R1} is about 4.35 × 10² at 298 K. Meanwhile, the H₂O · · HO₂ + SO₂ reaction can compete well with the HO₂ + NO₃ reaction because the rate ratio *v*_{a1}/*v*_{R2} is about 6.83 × 10³ at 298 K. Thus, compared with the primary loss mechanism of HO₂ radicals, the HO₂ + SO₂ → HOSO + ³O₂ reaction with H₂O cannot be neglected. Meanwhile, with increasing altitude, the values of *v*_{a1}/*v*_{R1} and *v*_{a1}/*v*_{R2} obviously decrease. At 218.6 K, the values of *v*_{a1}/*v*_{R1} and *v*_{a1}/*v*_{R2} are 5.22 × 10⁻⁴ and 1.73 × 10⁻³, showing that the HO₂ + SO₂ → HOSO + ³O₂ reaction with H₂O cannot compete with the primary loss mechanism of HO₂ radicals.

In order to test the competition of the H₂O · · HO₂ + SO₂ reaction with the primary loss mechanism of SO₂ (such as the

SO₂ + HO reaction), it is of great importance to discuss the rate ratio between H₂O · · HO₂ + SO₂ and SO₂ + OH, as shown in eqn (24).

$$\begin{aligned} \frac{v_{a1}}{v_{R3}} &= \frac{K_{eq}(\text{H}_2\text{O} \cdots \text{HO}_2)k_a(\text{WM1b})[\text{H}_2\text{O}][\text{HO}_2][\text{SO}_2]}{k_{R3}[\text{HO}][\text{SO}_2]} \\ &= \frac{K_{eq}(\text{H}_2\text{O} \cdots \text{HO}_2)k_a(\text{WM1b})[\text{H}_2\text{O}][\text{HO}_2]}{k_{R3}[\text{HO}]} \end{aligned} \quad (24)$$

Here, *k*_{R3} is the rate constant of the SO₂ + OH reaction, which is obtained from Table 3. The rate ratio *v*_{a1}/*v*_{R3} depends on the H₂O, OH, and HO₂ concentrations in the atmosphere. At 298 K, when the concentration of water is at a relative humidity of 100%, OH is 7.73 × 10¹⁷ and 1 × 10⁶ molecules per cm³, respectively, and the gas-phase concentration of HO₂ is 3 × 10⁸ molecules per cm³, the H₂O · · HO₂ + SO₂ reaction can compete with the SO₂ + HO reaction, because the rate ratio *v*_{a1}/*v*_{R3} is about 6.20 at 298 K. Consequently, the hydrogen atom transfer processes of the H₂O · · HO₂ + SO₂ reaction are more obvious in the atmosphere during the day than those of the SO₂ + HO reaction. Meanwhile, when the OH concentration decreases to 1 × 10⁴ molecules per cm³ during the night,⁸⁰ the H₂O · · HO₂ + SO₂ reaction can compete well with the SO₂ + HO reaction because the rate ratio *v*_{a1}/*v*_{R3} is about 6.20 × 10² at 298 K. Thus, the H₂O · · HO₂ + SO₂ reaction can also make a contribution to the sink of SO₂ during the night under the conditions of OH (10⁴ molecules per cm³), HO₂ (molecules per cm³), and H₂O (molecules per cm³).

Table 3 Rate constants (cm³ per molecules per s) for H₂O₂ + O₂ formation from the HO₂ + HO₂ reaction (R1), HNO₃ + O₂ formation from the NO₃ + HO₂ reaction (R2) and HSO₃ formation from the SO₂ + OH reaction (R3) within the temperature range of 218.6–320.0 K

T (K)	<i>k</i> _{R1}	<i>v</i> _{a1} / <i>v</i> _{R1}	<i>k</i> _{R2}	<i>v</i> _{a1} / <i>v</i> _{R2}	<i>k</i> _{R3}	<i>v</i> _{a1} / <i>v</i> _{R3}	<i>v</i> _{a1} / <i>v</i> _{R3(night)}
218.6	1.38 × 10 ⁻¹⁰	5.22 × 10 ⁻⁴	5.06 × 10 ⁻¹⁰	1.74 × 10 ⁻³	2.06 × 10 ⁻¹²	3.15 × 10 ⁻³	3.15 × 10 ⁻¹
223.7	8.29 × 10 ⁻¹¹	8.24 × 10 ⁻⁴	2.55 × 10 ⁻¹⁰	1.09 × 10 ⁻³	2.09 × 10 ⁻¹²	3.27 × 10 ⁻⁴	3.27 × 10 ⁻²
229.7	4.69 × 10 ⁻¹¹	1.63 × 10 ⁻¹	1.22 × 10 ⁻¹⁰	2.55 × 10 ⁻¹	2.14 × 10 ⁻¹²	3.58 × 10 ⁻²	3.58 × 10 ⁰
235.1	2.88 × 10 ⁻¹¹	4.54 × 10 ⁻⁴	6.72 × 10 ⁻¹¹	7.92 × 10 ⁻⁴	2.20 × 10 ⁻¹²	5.95 × 10 ⁻⁵	5.95 × 10 ⁻³
249.9	8.50 × 10 ⁻¹¹	2.53 × 10 ⁻³	1.68 × 10 ⁻¹¹	5.20 × 10 ⁻²	2.32 × 10 ⁻¹²	9.26 × 10 ⁻⁴	9.26 × 10 ⁻²
259.3	4.22 × 10 ⁻¹¹	1.02 × 10 ⁰	8.20 × 10 ⁻¹²	2.13 × 10 ¹	2.37 × 10 ⁻¹²	1.82 × 10 ⁻¹	1.82 × 10 ¹
280.0	1.08 × 10 ⁻¹¹	1.27 × 10 ¹	2.32 × 10 ⁻¹²	2.41 × 10 ²	2.53 × 10 ⁻¹²	5.43 × 10 ⁻¹	5.43 × 10 ¹
290.0	6.01 × 10 ⁻¹²	2.53 × 10 ¹	1.42 × 10 ⁻¹²	4.35 × 10 ²	2.64 × 10 ⁻¹²	5.76 × 10 ⁻¹	5.76 × 10 ¹
298.2	3.85 × 10 ⁻¹²	4.35 × 10 ²	9.96 × 10 ⁻¹³	6.83 × 10 ³	2.70 × 10 ⁻¹²	6.20 × 10 ⁰	6.20 × 10 ²
300.0	3.49 × 10 ⁻¹²	4.88 × 10 ²	9.23 × 10 ⁻¹³	7.51 × 10 ³	2.71 × 10 ⁻¹²	6.29 × 10 ⁰	6.29 × 10 ²
310.0	2.11 × 10 ⁻¹²	8.88 × 10 ²	6.29 × 10 ⁻¹³	1.21 × 10 ⁴	2.79 × 10 ⁻¹²	6.72 × 10 ⁰	6.72 × 10 ²
320.0	1.32 × 10 ⁻¹²	1.53 × 10 ²	4.46 × 10 ⁻¹³	1.84 × 10 ³	2.90 × 10 ⁻¹²	6.95 × 10 ⁻¹	6.95 × 10 ¹



4. Summary and conclusions

In this article, the hydrogen atom transfer processes of the $\text{HO}_2 + \text{SO}_2 \rightarrow \text{HOSO} + {}^3\text{O}_2$ reaction without and with $(\text{H}_2\text{O})_n$ ($n = 1\text{--}3$) have been investigated using the CCSD(T)/CBS//M06-2X/aug-cc-pVTZ method and canonical variational transition state theory with small curvature tunneling (CVT/SCT). The calculated results show that, for the $(\text{H}_2\text{O})_n$ ($n = 1\text{--}3$) + $\text{HO}_2 + \text{SO}_2$ reaction, the main entrance channel is the reaction of the $\text{HO}_2\cdots(\text{H}_2\text{O})_n$ ($n = 1\text{--}3$) complex with SO_2 . Additionally, H_2O exerts the strongest catalytic influence in the hydrogen atom transfer processes of the $\text{HO}_2 + \text{SO}_2 \rightarrow \text{HOSO} + {}^3\text{O}_2$ reaction compared with $(\text{H}_2\text{O})_2$ and $(\text{H}_2\text{O})_3$, which is due to the fact that the effective rate constant of the $\text{HO}_2\cdots\text{H}_2\text{O} + \text{SO}_2$ reaction is 2–3 and 4–6 orders of magnitude larger than the corresponding rate constants of the $\text{HO}_2\cdots(\text{H}_2\text{O})_2 + \text{SO}_2$ and $\text{HO}_2\cdots(\text{H}_2\text{O})_3 + \text{SO}_2$ reactions, respectively.

In the gas-phase reactions of the atmosphere, the importance of the $\text{HO}_2\cdots\text{H}_2\text{O} + \text{SO}_2$ reaction depends on its competition with the $\text{HO}_2 + \text{SO}_2 \rightarrow \text{HOSO} + {}^3\text{O}_2$ reaction. We show that, at 0 km altitude within the temperature range of 275–320 K, the effective rate constant of the $\text{HO}_2\cdots\text{H}_2\text{O} + \text{SO}_2$ reaction was 2–3 orders of magnitude larger than that of the $\text{HO}_2 + \text{SO}_2 \rightarrow \text{HOSO} + {}^3\text{O}_2$ reaction without a catalyst, indicating that the water monomer plays an obvious positive role in increasing the rate of the $\text{HO}_2 + \text{SO}_2 \rightarrow \text{HOSO} + {}^3\text{O}_2$ reaction. Compared with the primary loss mechanism of HO_2 radicals and SO_2 , the $\text{HO}_2 + \text{SO}_2 \rightarrow \text{HOSO} + {}^3\text{O}_2$ reaction with H_2O cannot be neglected with its rate constant close to the rate constant of those reactions of $\text{HO}_2 + \text{HO}_2$, $\text{HO}_2 + \text{NO}_3$ and $\text{SO}_2 + \text{HO}$. In addition, with the altitude increase, for the formation of $\text{HOSO} + {}^3\text{O}_2$, the contribution of H_2O decreases from 99.98% to 27.27% at the lower relative concentration of water, which indicates that the $\text{HO}_2\cdots\text{H}_2\text{O} + \text{SO}_2$ reaction cannot compete with the primary loss processes of HO_2 radicals and SO_2 at higher altitudes.

The findings of the present work not only show a specific $(\text{H}_2\text{O})_n$ ($n = 1\text{--}3$) catalyzed reaction for its reaction mechanism and kinetics, but also show that H_2O can obviously promote the hydrogen atom transfer processes of the $\text{HO}_2 + \text{SO}_2 \rightarrow \text{HOSO} + {}^3\text{O}_2$ reaction. Thus, the present investigation has wide applications in the hydrogen atom transfer processes of atmospheric processes, such as $\text{HO}_2 + \text{HO}_2$ and $\text{HO}_2 + \text{NO}_3$ reactions.

Conflicts of interest

There are no conflicts to declare.

Acknowledgements

This work was supported by the National Natural Science Foundation of China (No. 21603132, 41805107), the Project of Education Department in Shaanxi (18JK0147) and the Funds of Research Programs of Shaanxi University of Technology (No. SLGQD13(2)-3, SLGQD13(2)-4).

References

1 C. N. Hewitt, *Atmos. Environ.*, 2011, **35**, 1155–1170.

- 2 B. Long, J. L. Bao and D. G. Truhlar, *Phys. Chem. Chem. Phys.*, 2017, **19**, 8091–8100.
- 3 X. Chen, C. Tao, L. Zhong, Y. Gao, W. Yao and S. Li, *Chem. Phys. Lett.*, 2014, **608**, 272–276.
- 4 J. Liu, S. Fang, Z. Wang, W. Yi, F. M. Tao and J. Liu, *Environ. Sci. Technol.*, 2015, **49**, 13112–13120.
- 5 M. R. Rd, T. Berndt, M. Sipilä, P. Paasonen, T. Petäjä, S. Kim, T. Kurtén, F. Stratmann, V. M. Kerminen and M. Kulmala, *Nature*, 2012, **488**, 193.
- 6 R. Zhang, A. Khalizov, L. Wang, M. Hu and W. Xu, *Chem. Rev.*, 2011, **112**, 1957–2011.
- 7 N. Sang, Y. Yun, G. Y. Yao, *et al.*, *Toxicol. Sci.*, 2011, **124**, 400–413.
- 8 Y. Tang, G. S. Tyndall and J. J. Orlando, *J. Phys. Chem. A*, 2010, **114**, 369–378.
- 9 P. D. Lightfoot, R. A. Cox, J. N. Crowley, M. Destriau, G. D. Hayman, M. E. Jenkin, G. K. Moortgat and F. Zabel, *Atmos. Environ.*, 1992, **26**, 1805–1961.
- 10 D. Stone, L. K. Whalley and D. E. Heard, *Chem. Soc. Rev.*, 2012, **41**, 6348–6404.
- 11 B. Wang and H. Hou, *Phys. Lett.*, 2005, **410**, 235–241.
- 12 S. E. Wheeler, *J. Phys. Chem. A*, 2009, **113**, 6779–6788.
- 13 A. Lesar and A. Tavčar, *J. Phys. Chem. A*, 2011, **115**, 11008–11015.
- 14 A. J. Frank, M. Sadílek, J. G. Ferrier and F. E. Tureček, *J. Am. Chem. Soc.*, 1996, **118**, 11321–11322.
- 15 E. Isoniemi, L. Khriachtchev, J. Lundell and M. Räsänen, *J. Mol. Struct.*, 2001, **563**, 261–265.
- 16 R. J. Boyd, A. Gupta, R. F. Langler, S. P. Lownie and J. A. Pincock, *Can. J. Chem.*, 1980, **58**, 331–338.
- 17 M. C. McCarthy, V. Lattanzi, J. Oscar Martinez and F. E. Tureček, *J. Phys. Chem. Lett.*, 2013, **4**, 4074–4079.
- 18 Y. Q. Sun, X. Wang, F. Y. Bai and X. M. Pan, *Environ. Chem.*, 2017, **14**, 19–30.
- 19 W. A. Payne, L. J. Stief and D. D. Davis, *J. Am. Chem. Soc.*, 1973, **95**, 7614–7619.
- 20 J. P. Burrows, D. I. Cliff, G. W. Harris, B. A. Thrush and J. P. T. Wilkinson, *Proc. R. Soc. London, Ser. A*, 1979, **368**, 463–481.
- 21 R. J. Buszek, J. S. Francisco and J. M. Anglada, *Int. Rev. Phys. Chem.*, 2011, **30**, 335–369.
- 22 T. Zhang, W. Wang, P. Zhang, J. Lü and Y. Zhang, *Phys. Chem. Chem. Phys.*, 2011, **13**, 20794–20805.
- 23 R. J. Buszek, M. Torrentsucarrat, J. M. Anglada and J. S. Francisco, *J. Phys. Chem. A*, 2012, **116**, 5821–5829.
- 24 J. M. Anglada and J. Gonzalez, *ChemPhysChem*, 2009, **10**, 3034–3045.
- 25 J. Gonzalez and J. M. Anglada, *J. Phys. Chem. A*, 2010, **114**, 9151–9162.
- 26 J. Gonzalez, J. M. Anglada, R. J. Buszek and J. S. Francisco, *J. Am. Chem. Soc.*, 2011, **133**, 3345–3353.
- 27 J. C. Hansen and J. S. Francisco, *ChemPhysChem*, 2002, **3**, 833–840.
- 28 V. Vaida, H. G. Kjaergaard, P. E. Hintze and D. J. Donaldson, *Science*, 2003, **299**, 1566–1568.
- 29 N. Kanno, K. Tonokura, A. Tezaki and M. Koshi, *J. Phys. Chem. A*, 2005, **109**, 3153–3158.



30 K. Suma, Y. Sumiyoshi and Y. Endo, *Science*, 2006, **311**, 1278–1281.

31 N. Butkovskaya, M. T. Rayez, J. C. Rayez, A. Kukui and G. L. Bras, *J. Phys. Chem. A*, 2009, **113**, 11327–11342.

32 S. Aloisio, J. S. Francisco and R. R. Friedl, *J. Phys. Chem. A*, 2000, **104**, 6597–6601.

33 J. Liu, S. Fang, W. Liu, A. Kukui and G. L. Bras, *J. Phys. Chem. A*, 2015, **119**, 102–111.

34 T. L. Tarbuck and G. L. Richmond, *J. Am. Chem. Soc.*, 2005, **127**, 16806–16807.

35 T. L. Tarbuck and G. L. Richmond, *J. Am. Chem. Soc.*, 2006, **128**, 3256–3267.

36 S. T. Ota and G. L. Richmond, *J. Am. Chem. Soc.*, 2011, **133**, 7497–7508.

37 K. Matsumura, F. J. Lovas and R. D. Suenram, *J. Chem. Phys.*, 1989, **91**, 5887–5894.

38 T. Zhang, C. Yang, X. Feng, J. Kang, L. Song, Y. Lu, Z. Wang, Q. Xu, W. Wang and Z. Wang, *Phys. Chem. Chem. Phys.*, 2016, **18**, 17414–17427.

39 L. P. Viegas and A. J. C. Varandas, *Eur. Phys. J. D*, 2016, **70**, 48.

40 Y. P. Zhao and Y. P. Zeng, *Chin. J. Struct. Chem.*, 2010, **29**, 499–508.

41 R. Steudel and Y. Steudel, *Eur. J. Inorg. Chem.*, 2009, **2009**, 1393–1405.

42 B. Du and W. Zhang, *Comput. Theor. Chem.*, 2014, **1049**, 90–96.

43 E. Vöhringermartinez, B. Hansmann and H. Hernandezsoto, *Science*, 2007, **315**, 497–501.

44 R. Wang, J. Kang and S. Zhang, *Comput. Theor. Chem.*, 2017, **1110**, 25–34.

45 P. Kumar, P. Biswas and B. Bandyopadhyay, *Phys. Chem. Chem. Phys.*, 2016, **18**, 27728–27732.

46 B. Du and W. Zhang, *Comput. Theor. Chem.*, 2015, **1069**, 77–85.

47 L. P. Viegas and A. J. Varandas, *J. Phys. Chem. B*, 2016, **120**, 1560–1568.

48 J. M. Anglada, G. J. Hoffman, L. V. Slipchenko, M. M. Costa, M. F. Ruizlópez and J. S. Francisco, *J. Phys. Chem. A*, 2013, **117**, 10381–10396.

49 P. Miró and C. J. Cramer, *Phys. Chem. Chem. Phys.*, 2013, **15**, 1837–1843.

50 J. Hernández-Rojas and D. J. Wales, *Chem. Phys.*, 2014, **444**, 23–29.

51 E. A. Cobar, P. R. Horn, R. G. Bergman and M. Headgordon, *Phys. Chem. Chem. Phys.*, 2012, **14**, 15328–15339.

52 J. A. Anderson, K. Crager, L. Fedoroff and G. S. Tschumper, *J. Chem. Phys.*, 2004, **121**, 11023–11029.

53 M. E. Dunn, E. K. Pokon and G. C. Shields, *J. Am. Chem. Soc.*, 2004, **126**, 2647–2653.

54 N. Goldman, R. S. Fellers and C. Leforestier, *J. Phys. Chem. A*, 2001, **105**, 515–519.

55 Y. S. Lee, S. A. Kucharski and R. J. Bartlett, *J. Chem. Phys.*, 1985, **82**, 5761.

56 C. Gonzalez and H. B. Schlegel, *J. Chem. Phys.*, 1989, **90**, 2154–2161.

57 Y. S. Lee, S. A. Kucharski and R. J. Bartlett, *J. Chem. Phys.*, 1984, **81**, 5906–5912.

58 A. J. C. Varandas and F. N. N. Pansini, *J. Chem. Phys.*, 2014, **141**, 224113.

59 B. C. Garrett and D. G. Truhlar, *J. Chem. Phys.*, 1979, **70**, 1593–1598.

60 B. C. Garrett and D. G. Truhlar, *Chem. Informationsdienst*, 1979, **10**, 4534–4548.

61 B. C. Garrett, D. G. Truhlar, R. S. Grev and A. W. Magnuson, *J. Chem. Phys.*, 1980, **84**, 1730–1748.

62 D. H. Lu, T. N. Truong, S. G. Melissas, C. Lynch, Y. P. Liu and B. C. Garrett, *Comput. Phys. Commun.*, 1992, **71**, 235–262.

63 Y. P. Liu, G. C. Lynch, T. N. Truong, D. H. Lu, D. G. Truhlar and B. C. Garretet, *J. Am. Chem. Soc.*, 1993, **6**, 2408–2415.

64 S. W. Zhang and N. T. Truong, *VKLab, version 1.0*, University of Utah, Salt Lake City, 2001.

65 M. J. Frisch, G. W. Trucks and J. A. Pople, *Gaussian 09, Revision A.01*, Gaussian Inc., Pittsburgh, PA, 2009.

66 R. Atkinson, D. L. Baulch and R. A. Cox, *Atmos. Chem. Phys.*, 2004, **3**, 1461–1738.

67 R. J. Buszek, J. R. Barker and J. S. Francisco, *J. Phys. Chem. A*, 2012, **116**, 4712–4719.

68 X. Chen, Y. F. Zhao, L. S. Wang and J. Li, *Comput. Theor. Chem.*, 2017, **1107**, 57–65.

69 Y. Zhao, X. Chen and J. Li, *Nano Res.*, 2017, **10**, 3407–3420.

70 B. Long, X. F. Tan, Z. W. Long, Y. B. Wang, D. S. Ren and W. J. Zhang, *J. Phys. Chem. A*, 2011, **115**, 6559–6567.

71 T. Zhang, R. Wang, W. Wang, S. Min, Q. Xu, Z. Wang, C. Zhao and Z. Wang, *Comput. Theor. Chem.*, 2014, **1045**, 135–144.

72 J. Gonzalez, M. Torrent-Sucarrat and J. M. Anglada, *Phys. Chem. Chem. Phys.*, 2010, **12**, 2116–2125.

73 T. Zhang, W. Wang, C. Li and Y. Du, *RSC Adv.*, 2013, **3**, 7381–7391.

74 T. Zhang, R. Wang, H. Chen, S. Min, Z. Wang, C. Zhao, Q. Xu, L. Jin, W. Wang and Z. Wang, *Phys. Chem. Chem. Phys.*, 2015, **17**, 15046–15055.

75 S. Mallick, S. Sarkar, P. Kumar and B. Bandyopadhyay, *J. Phys. Chem. A*, 2018, **122**, 350–363.

76 A. Mellouki, R. K. Talukdar and A. M. R. P. Bopegedera, *Int. J. Chem. Kinet.*, 1993, **25**, 25–39.

77 D. Stone and D. M. Rowley, *Phys. Chem. Chem. Phys.*, 2005, **7**, 2156–2163.

78 E. Becker, M. M. Rahman and R. N. Schindler, *Ber. Bunsenges. Phys. Chem.*, 1992, **96**, 776–783.

79 D. Fulle, H. F. Hamann and H. Hippel, *Phys. Chem. Chem. Phys.*, 1999, **1**, 2695–2702.

80 M. A. H. Khan, M. J. Ashfold, G. Nickless, D. Martin, L. A. Watson, P. D. Hamer, R. P. Wayne, C. E. Canosa-Mas and D. E. Shallock, *Atmos. Sci. Lett.*, 2008, **9**, 140–146.

